

# An aluminum-based reflective nanolens array that enhances the effectiveness of a continuous-flow ultraviolet disinfection system for livestock water

Changhoon Chai\* and Jinhyung Park

Department of Applied Animal Science, Kangwon National University, Chuncheon 24341, Korea



Received: Aug 16, 2022

Revised: Oct 20, 2022

Accepted: Oct 28, 2022

## \*Corresponding author

Changhoon Chai

Department of Applied Animal Science, Kangwon National University, Chuncheon 24341, Korea.

Tel: +82-33-250-8641

E-mail: [chchai@kangwon.ac.kr](mailto:chchai@kangwon.ac.kr)

Copyright © 2023 Korean Society of Animal Sciences and Technology.

This is an Open Access article distributed under the terms of the Creative Commons Attribution Non-Commercial License (<http://creativecommons.org/licenses/by-nc/4.0/>) which permits unrestricted non-commercial use, distribution, and reproduction in any medium, provided the original work is properly cited.

## ORCID

Changhoon Chai

<https://orcid.org/0000-0003-4320-7311>

Jinhyung Park

<https://orcid.org/0000-0002-5513-3172>

## Competing interests

No potential conflict of interest relevant to this article was reported.

## Funding sources

This study was supported by a grant from the National Research Foundation of Korea (NRF-2019R111A3A01052210), funded by the Korean government.

## Abstract

Climate change has worsened droughts and floods, and created conditions more likely to lead to pathogen contamination of surface water and groundwater. Thus, there is a growing need to disinfect livestock water. Ultraviolet (UV) irradiation is widely accepted as an appropriate method for disinfecting livestock water, as it does not produce hazardous chemical compounds and kills pathogens. However, UV-based disinfection inevitably consumes electricity, so it is necessary to improve UV disinfection effectiveness. Aluminum-based reflective nanolens arrays that enhanced the effectiveness of a continuous-flow UV water disinfection system were developed using electrochemical and chemical processes, including electropolishing and two-step anodization. A continuous UV disinfection system was custom designed and the parts were produced using a three-dimensional printer. Electropolished aluminum was anodized at 40 and 80 V in 0.3 M oxalic acid, at 120 and 160 V in 1.0 M phosphoric acid, and at 200 and 240 V in 1.5 M citric acid. The average nanolens diameters ( $D$ ) of the aluminum-based reflective nanolens arrays prepared using 40, 80, 120, 160, 200, and 240 V anodization were 95.44, 160.98, 226.64, 309.90, 296.32, and 339.68 nm, respectively. Simple UV reflection behind irradiated water disinfected *Escherichia coli* O157:H7 in water more than did the non-reflective control. UV reflection and focusing behind irradiated water using an aluminum-based reflective nanolens array disinfected *E. coli* O157:H7 more than did simple UV reflection. Such enhancement of the UV disinfection effectiveness was significantly effective when a nanolens array with  $D$  226.64 nm, close to the wavelength of the irradiated UV (254 nm), was used.

**Keywords:** Nanolens array, UV inactivation, Anodic aluminum oxide, Livestock water

## INTRODUCTION

An adequate supply of clean and safe water is critical for producing safe and healthy livestock and poultry [1,2]. Livestock and poultry may be given water originating from surface water (e.g., streams, rivers, lakes, etc.), rainwater, or groundwater (e.g., underground springs and wells) [3,4]. Microbiological

**Acknowledgements**

We thank Sunmi Han for her assistance.

**Availability of data and material**

Upon reasonable request, the datasets of this study can be available from the corresponding author.

**Authors' contributions**

Conceptualization: Chai C.  
Data curation: Chai C, Park J.  
Formal analysis: Chai C, Park J.  
Methodology: Chai C.  
Software: Chai C.  
Validation: Chai C, Park J.  
Investigation: Chai C.  
Writing - original draft: Chai C, Park J.  
Writing - review & editing: Chai C, Park J.

**Ethics approval and consent to participate**

This article does not require IRB/ACUC approval because there are no human and animal participants.

contamination of livestock water is highly correlated with the microbiological safety of livestock products [5,6]. Microbiologically hazardous livestock water should be disinfected. However, the global temperature has been increasing for over 100 years [7], and the severity and likelihood of droughts and floods have increased worldwide [8]; this has reduced the surface water available for livestock, and has even caused pathogen contamination of groundwater [9]. There is a growing need to disinfect livestock water due to climate change.

Livestock water may be chlorinated, filtered, ozonated, or ultraviolet (UV)-irradiated to ensure microbiological safety. Chlorination is easy and effective, and the most common water treatment method [3]. However, chlorination produces disinfection by-products (DBPs) through the interactions of chlorine with organic matter naturally present in water. DBPs include genotoxic, mutagenic, and carcinogenic compounds such as dichloroacetic acid, chlorophenols, and trihalomethanes [10,11]. DBPs increase the risk of various cancers in humans [12], and cause health and reproductive problems in livestock and poultry [13]. UV-based water treatment is widely accepted as an alternative to chlorination, because it effectively inactivates pathogenic microorganisms but does not require chemicals or generate DBPs [14]. UV-based water treatment is rapidly gaining popularity. The global UV disinfection equipment market was USD 1.3 billion in 2019 and is estimated to reach USD 5.7 billion by 2027, with a mean annual growth rate of 17.1% projected from 2020 to 2027 [15]. However, UV-based water treatment inevitably consumes electricity, putting economic strain on farmers and environmental burden on the climate. Therefore, it is necessary to develop an energy-efficient UV water disinfection system. Enhancing UV disinfection effectiveness may improve the energy efficiency of UV water disinfection systems as processing capacity changes, which is the motivation for this study.

UV is electromagnetic radiation at wavelengths of 10–400 nm and has germicidal activity. When microorganisms in water are irradiated with UV, the microbial DNA is damaged, which hinders RNA synthesis and DNA replication, and inactivates the microorganisms. The germicidal activity of UV is directly related to the UV dose, which depends on the period of UV irradiation [16,17]. Longer exposure to UV causes greater DNA damage and decreased viability of *Escherichia coli* [17]. The total UV dose received by microorganisms in water can be increased (without supplying additional UV) by placing a reflector behind the object to be irradiated; this enhances UV disinfection effectiveness [18,19]. In addition, UV, like other light, can be focused to a point by a lens. Microorganisms are readily inactivated by focused UV [19]. Therefore, we supposed that UV water disinfection effectiveness would be enhanced if UV was reflected and focused on microorganisms by a reflector placed behind the water. When developing reflective concave lenses to enhance UV water disinfection effectiveness, we considered the size and distribution of microorganisms in water. Microorganisms that contaminate water include viruses (20–1,000 nm in size), bacteria (1–8  $\mu\text{m}$ ), and protozoa (10–50  $\mu\text{m}$ ) and are randomly distributed in water [20,21]. We hypothesized that an array of reflective concave lenses with a submicrometer inter-lens distance would allow UV light reflected behind the water to be focused on randomly distributed microorganisms, enhancing the UV disinfection effectiveness.

Aluminum is highly reflective, but reflectivity is affected by surface roughness. An aluminum surface can be electropolished to a mirror-like state as aluminum is electrochemically reactive [22]. In addition, via anodization, the aluminum surface can be fabricated into a nanoporous structure (with hexagonally arranged nanopores) by applying an electrical voltage under acidic conditions. In this process, when aluminum is oxidized, an aluminum oxide layer develops on the surface but is then partially corroded to produce a nanoporous aluminum oxide layer (Fig. 1) [23]. The anodic aluminum oxide (AAO) layer consists of hexagonal AAO cells (Fig. 1B). A cylindrical nanopore with a round bottom forms in the center of each AAO cell [24]. The sizes of the AAO cells and

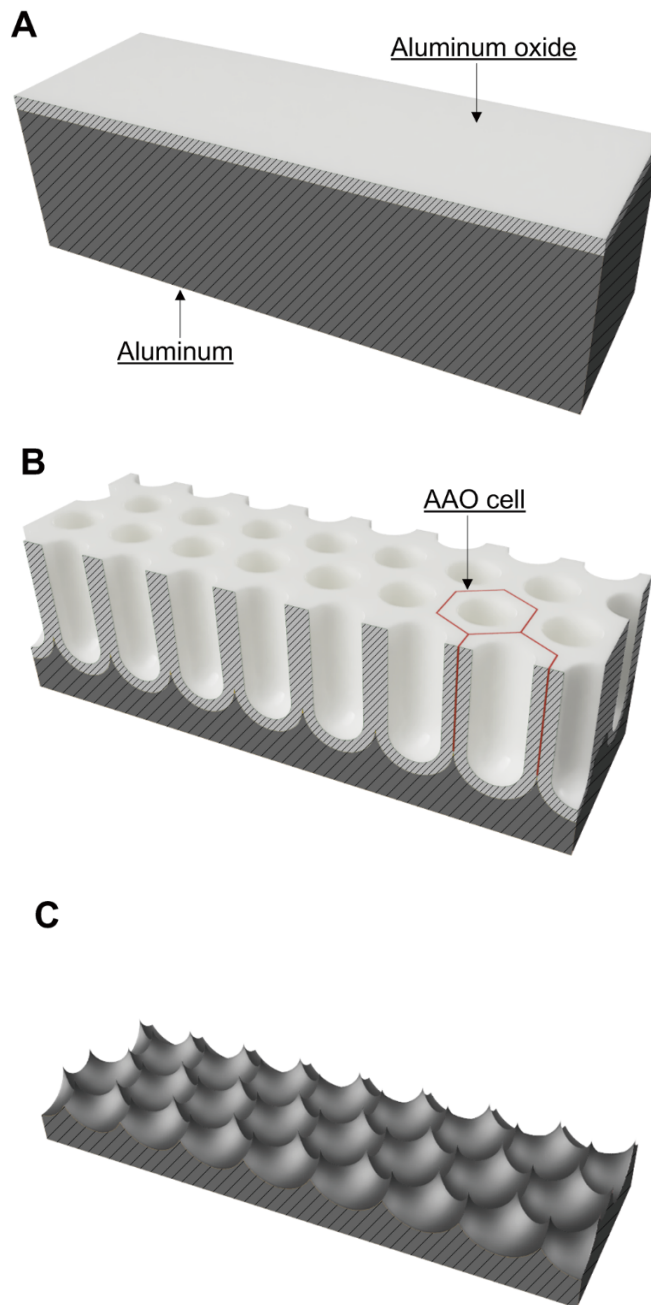


**Fig. 1.** Schematics of (A) electropolished aluminum, (B) a porous aluminum oxide layer on anodic aluminum, and (C) an aluminum-based nanolens array. AAO, anodic aluminum oxide.

nanopores depend on the electrolyte and voltage used for anodization [25]. Aluminum anodization yields ordered porous AAO layers of various cell diameters under different conditions, for example, oxalic acid at 40–70 V (50–100 nm) [26], phosphoric acid at 100–195 V (250–380 nm) [25], and citric acid at 200–370 V (500 nm) [27,28]. Beneath the AAO cell, the aluminum is concave. Thus, a regularly arranged nanolens array can be obtained by removing the AAO layer in a chemical solution selectively reactive to AAO (Fig. 1C).

We postulated that UV disinfection effectiveness could be enhanced using aluminum-based

reflective nanolens arrays. In particular, we investigated the effects of the array lens diameter ( $D$ ) on UV disinfection. Aluminum-based reflective nanolens arrays with  $D$  values of 95–330 nm were developed via electrochemical and chemical processes. A continuous-flow UV disinfection system that placed an aluminum-based reflective nanolens array in direct contact with water was custom-designed and -developed. *E. coli* O157:H7-inoculated water was treated with the custom-made system equipped with an aluminum-based reflective nanolens array, and viable *E. coli* O157:H7 were counted. Based on the UV disinfection test, we explored the effects of  $D$  on UV disinfection and nanolens arrays that enhanced the effectiveness of the UV water disinfection system.

## MATERIALS AND METHODS

### Materials

Aluminum sheets (alloy 1050), quartz plates, and graphite cathodes were purchased from Kwang-Lim Metal (Hwaseong, Korea), Seoul Special Glass (Namyangju, Korea), and Moon Hwa Titan Art (Incheon, Korea), respectively. Acetone (all v/v) (99.8%), chromic acid (99%), citric acid (99.5%), ethanol (99.5%), and perchloric acid (90%) were purchased from Daejung Chemicals and Metals (Siheung, Korea). Ethylene glycol (99.5%) and oxalic acid (99.5%) were purchased from Junsei Chemical (Tokyo, Japan). Phosphoric acid (85%) was purchased from Sigma-Aldrich (St. Louis, MO, USA). Luria-Bertani (LB) broth and LB agar were purchased from BD (Sparks, MD, USA). Hexagonal head bolts (size: M5 × 40 mm) and butterfly nuts (size: M5) were purchased from a local market.

### Methods

#### *Preparation of nanolens arrays*

Nanolens arrays were prepared via two-step anodization with subsequent chemical dissolution of AAO. Industrial-grade 180 × 30 × 1 mm aluminum sheets were cleaned with acetone, annealed at 400 °C for 2 h, and cooled slowly to ambient temperature. The aluminum was electropolished by applying 42 V for 40 s at 5 °C in a solution of ethanol, ethylene glycol, perchloric acid, and distilled water (DW) (71:10:7:12 by volume) using an electrochemical reactor featuring a DC power supply (TEX-300, Toyotech, Incheon, Korea), an anode clamp, a graphite cathode (180 × 30 × 4 mm), a jacketed beaker, and a circulating constant temperature bath (CCA-112A, Eyela, Tokyo, Japan). The electropolished aluminum was washed vigorously with DW and dried at 60 °C.

Two-step anodization featured initial anodization followed by chemical dissolution of AAO and second anodization and dissolution steps. The electrochemical reactor described above was also used for anodization. The first anodization was conducted at 40 and 80 V in 0.3 M oxalic acid, 120 and 160 V in 1.0 M phosphoric acid, and 200 and 240 V in 1.5 M citric acid for 20 min each. During anodization, the solution temperature was maintained below 5 °C. Anodized aluminum was washed with DW, dried, placed in a solution of 0.15 M chromic acid and 0.6 M phosphoric acid for 8 h at 65 °C to remove AAO, washed with DW, and dried. The second anodization was performed for 10 min using the same voltage and solution as the first anodization, and the anodized aluminum was washed and dried. Aluminum-based reflective nanolens arrays were produced by chemically removing the AAO formed by the second anodization. The second AAO dissolution was performed as for the first dissolution. The aluminum-based reflective nanolens arrays were washed with DW, dried, and then kept in 99.5% (v/v) ethanol and dried. The nanolens arrays were irradiated with germicidal UV (254 nm; 8 W; G8T5; Sankyo Denski, Hiratsuka, Kanagawa, Japan) for 1 h and stored in a sterile container until use.

### Nanolens array surface geometries

The surface geometries of nanolens arrays were analyzed using a scanning probe microscope (Easyscan 2, Nanosurf AG, Liestal, Switzerland). The surface geometric parameters were obtained in tapping mode using a FortA silicon probe with a nominal spring constant of 1.6 N/m (Applied NanoStructures, Mountain View, CA, USA). Scanning probe image processor software (SPIP, Image Metrology, Lyngby, Denmark) was used to process surface images and obtain  $D$  values. The  $D$  values were compared by one-way analysis of variance followed by Scheffé's *post-hoc* test ( $p < 0.05$ ) with SPSS ver. 26 software (IBM, Armonk, NY, USA).

### Nanolens array-equipped continuous-flow UV water disinfection system

A nanolens array-equipped continuous-flow UV water disinfection system was designed using three-dimensional (3D) modeling software (Fusion 360, Autodesk, San Rafael, CA, USA). The system featured a quartz plate holder, a UV reactor body with liquid inlet and outlet ports, a nanolens array holder, a quartz plate (180 × 30 × 2 mm), a nanolens array, and silicone spacers (thickness 2 mm) (Figs. 2A and 2B). The volumetric capacity of the system holding the water to be irradiated by UV was approximately 39 mL. The 3D models of a quartz plate holder, a UV reactor body, and a nanolens array holder were sent to an on-demand 3D printing service company (Crello, Seoul, Korea) and printed using acrylonitrile butadiene styrene employing a stereolithographic 3D printer (the details of the 3D printing conditions were not provided by the company). All components were maintained in 99.5% (v/v) ethanol for 1 h, dried, irradiated with germicidal UV for 1 h, and stored in a sterile container until use. Before the UV disinfection test, the UV disinfection system was assembled using hexagon head bolts and butterfly nuts (Fig. 2C).

### Preparation of pathogen-contaminated water

*E. coli* O157:H7 ATCC 35150 (American Type Culture Collection, Rockville, MD, USA) served as a model water contaminant. The *E. coli* O157:H7-contaminated water was freshly prepared before the UV disinfection test. *E. coli* O157:H7 was cultured in LB broth. Cultures were centrifuged at 5,000×g for 20 min. The cell pellet was collected, washed with sterilized DW, resuspended in sterilized DW, and diluted to 5–6 log CFU mL<sup>-1</sup>.

### UV disinfection test

The UV disinfection system featuring an aluminum-based reflective nanolens array was connected to a peristaltic pump (PL-PP150D, Poong Lim, Seoul, Korea) using tubing. The system was placed on a jack lift table and covered with a custom-made UV safety box with a UV lamp slot. A germicidal UV lamp (254 nm; 8 W; G8T5; Sankyo Denski, Kanagawa, Japan) was mounted on the slot. The distance between the UV lamp and the quartz plate of the UV disinfection system was adjusted to 65 mm, corresponding to a UV intensity of 2.072 mW cm<sup>-2</sup>. The UV intensity at 254 nm was measured using a UV radiometer (VLX-3, Vilber Lourmat, Marine, France) fitted with a CX-254 sensor (Vilber Lourmat). *E. coli* O157:H7-contaminated water was fed to the system as UV was irradiated. Water from the system was collected, diluted, and plated onto LB agar plates. Viable *E. coli* O157:H7 numbers were enumerated after incubation of the LB agar plates at 37°C for 24 h. A graphite plate (180 × 30 × 4 mm) served as a control. To avoid unwanted photochemical reactions between UV and the graphite plate, a quartz plate (180 × 30 × 2 mm) was placed over the graphite plate. The UV disinfection test was performed in triplicate, once each for three aluminum-based reflective nanolens arrays prepared under identical conditions. The numbers of viable *E. coli* O157:H7 after UV treatment were compared by one-way analysis of variance followed by Tukey's *post-hoc* test ( $p < 0.05$ ) with SPSS ver. 26 software.

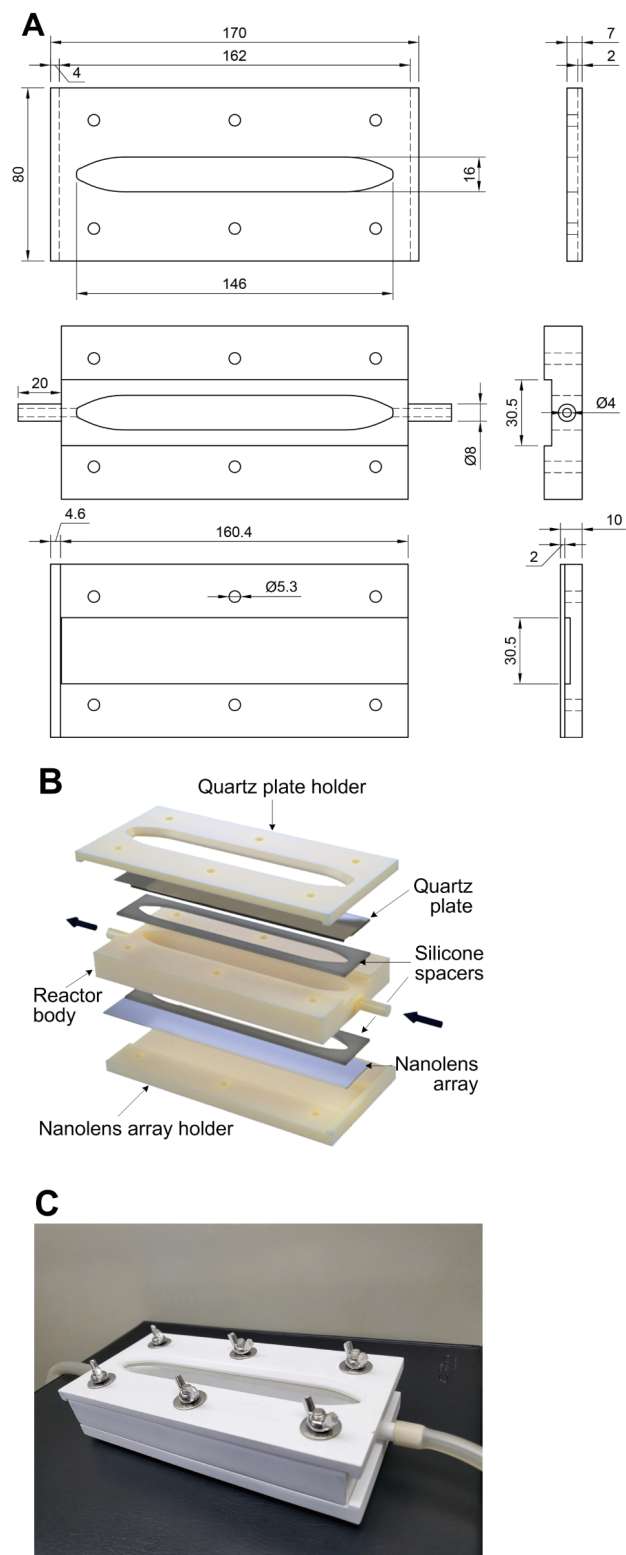


**Fig. 2.** The continuous-flow UV disinfection system with aluminum-based reflective nanolens arrays. (A) The 2D design, (B) the system configuration, and (C) a photograph of the system.

## RESULTS AND DISCUSSION

### Development of aluminum-based reflective nanolens arrays

The aluminum used (alloy 1050; aluminum purity 99.5%) was provided in a mechanically finished form. Electropolishing smoothed the rough aluminum surface to a mirror-like surface (Figs. 3A and 3B). Via anodization at 120 V in 1.0 M phosphoric acid, AAO developed as the aluminum was partially dissolved, and a nanoporous AAO layer formed on the surface (Fig. 3C). A nanolens array was obtained by removing the AAO (Fig. 3D). A second anodization followed by AAO removal was also performed. Finally, the nanolens arrays were obtained (Fig. 4). The arrays prepared via two-step anodization evidenced more ordered structures than those after one-step anodization (Figs. 3D and 4C). Thus, nanolens arrays prepared via two-step anodization were used for further study.

The average  $D$  values of arrays prepared via 40, 80, 120, 160, 200, and 240 V anodization were 95.44, 160.98, 226.64, 309.90, 296.32, and 339.68 nm, respectively (Fig. 5). Although the anodization voltage was higher, the  $D$  of the nanolens array prepared via 200 V anodization was not greater than that after 160 V anodization (Fig. 5). The  $D$  values we obtained were smaller than those reported previously [25,27,28]. We could not raise the anodization voltage to above 80 V in 0.3 M oxalic acid, above 160 V in 1.0 M phosphoric acid, or above 240 V in 1.5 M citric acid because the solution temperatures increased to levels that created burn defects. The cathode (graphite)-to-anode area ratio for the anodization in this study was approximately unity to facilitate uniform nanolens array fabrication. The cathode-to-anode area ratio affects the local electrical

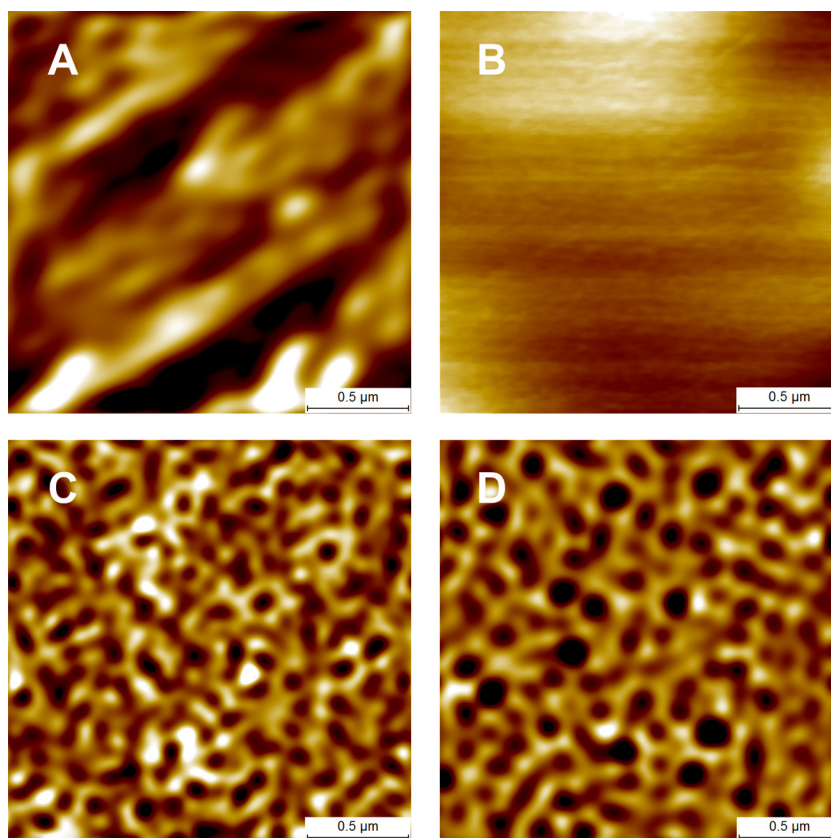


**Fig. 3.** SPM surface images of (A) bare aluminum, (B) electropolished aluminum, (C) anodized aluminum (after the first anodization at 120 V in 1.0 M phosphoric acid), and (D) AAO-free anodic aluminum (after the first AAO removal). SPM, scanning probe microscope; AAO, anodic aluminum oxide.

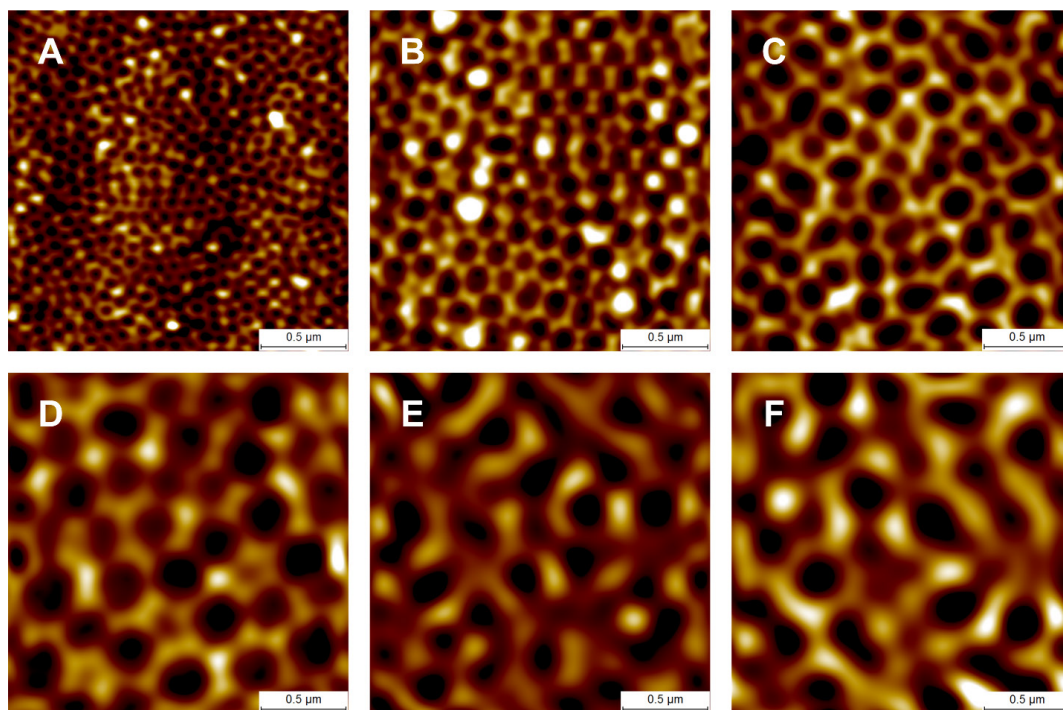


**Fig. 4.** SPM surface images of nanolens arrays prepared via two-step anodization at (A) 40, (B) 80, (C) 120, (D) 160, (E) 200, and (F) 240 V. SPM, scanning probe microscope.

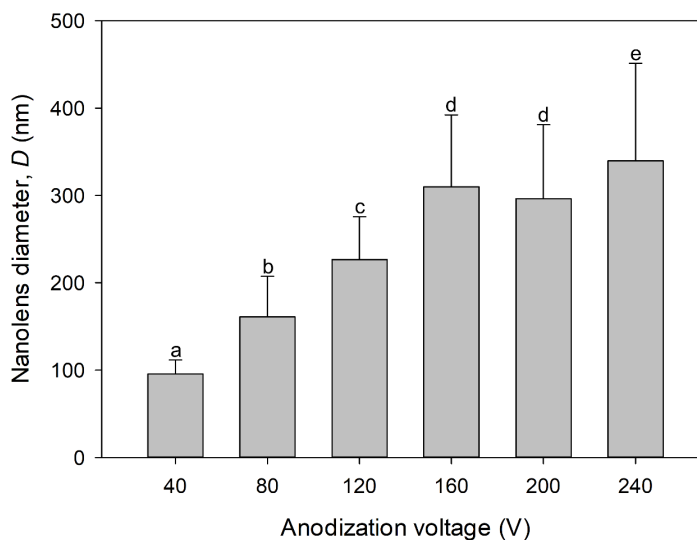


**Fig. 5.** The nanolens diameters ( $D$  values) of the aluminum-based, reflective nanolens arrays. Different letters above the error bars indicate significant differences ( $p < 0.05$ ) among the groups.

current density on AAO during anodization [29]. Higher cathode-to-anode ratios indicate greater local electrical current densities and larger AAO cells [29,30]. The differences in the  $D$  values between the present and other studies may be attributable to differences in the cathode-to-anode area ratios.

### Aluminum-based nanolens arrays enhancing UV disinfection effectiveness

UV irradiation becomes more intense as the distance between the UV lamp and the irradiated body decreases. The closest distance between the UV lamp and the quartz plate of the UV disinfection system was 8 mm, at which point the UV intensity was  $7.452 \text{ mW cm}^{-2}$ . No viable *E. coli* O157:H7 were found after the UV disinfection test under any conditions when the UV disinfection test was performed at 8 mm. The distance between the UV lamp and the quartz plate was adjusted to 65 mm (UV intensity  $2.075 \text{ mW cm}^{-2}$ ), and we performed UV disinfection tests of *E. coli* O157:H7-contaminated water flowing into the system at 1.5, 2, and  $4 \text{ mL s}^{-1}$ , which enabled us to obtain statistically significant results.

The UV energy imparted to the system should be equivalent when the control (graphite plate), electropolished aluminum, and aluminum-based reflective nanolens arrays were present. Graphite efficiently absorbs light, especially UV light [31]. Thus, the differences in UV disinfection results were attributable to UV reflection and focusing (Fig. 6). The *E. coli* O157:H7 was inactivated, and the count decreased from 5.74 to  $2.69 \text{ log CFU mL}^{-1}$  when UV irradiation was delivered at an *E. coli* O157:H7-contaminated water at  $2 \text{ mL s}^{-1}$  (Fig. 6A). After disinfection using the electropolished aluminum-equipped UV disinfection system (flow rate  $2 \text{ mL s}^{-1}$ ), the *E. coli* O157:H7 number fell to  $2.00 \text{ log CFU mL}^{-1}$ , significantly different from the control value (Fig. 6A). The total UV energy reaching *E. coli* O157:H7 in the system equipped with electropolished aluminum might have been greater than that of the control because the *E. coli* O157:H7 numbers fell more when the electropolished aluminum was employed. The *E. coli* O157:H7 level further decreased when aluminum-based reflective nanolens arrays (rather than electropolished aluminum) were used (Fig. 6A). In particular, after UV disinfection at  $2 \text{ mL s}^{-1}$  using nanolens arrays prepared via 80, 120, and 200 V anodization, the *E. coli* O157:H7 levels decreased from 5.74 to 1.64, 1.36, and  $1.74 \text{ log CFU mL}^{-1}$ , respectively (Fig. 6A). As no significant difference was apparent (Fig. 6A), the UV disinfection of nanolens arrays prepared via 80, 120, and 200 V anodization were tested at a flow rate of  $4 \text{ mL s}^{-1}$  (Fig. 6B). The *E. coli* O157:H7 numbers fell maximally when arrays prepared via 120 V anodization were used, with significantly lower numbers than those of 80 and 200 V anodization (Fig. 6B). No viable *E. coli* O157:H7 were found after UV disinfection at a flow rate of  $1.5 \text{ mL s}^{-1}$  using aluminum-based reflective nanolens arrays prepared via 120 V anodization. However, viable *E. coli* O157:H7 remained after disinfection at  $1.5 \text{ mL s}^{-1}$  in the control and electropolished aluminum tests (Fig. 6C). The UV disinfection tests revealed that the UV disinfection effectiveness could be enhanced using the aluminum-based reflective nanolens arrays and might be affected by  $D$  (Figs. 5 and 6).

UV reflection and focusing onto *E. coli* O157:H7 using the aluminum-based reflective nanolens arrays can enhance UV disinfection effectiveness. The surface structure of the nanolens array may affect UV disinfection. Light reflection is specular rather than diffuse when light is sent to a reflector with surface protrusions smaller than the wavelength [32]. We used a UV lamp mainly emitting 254 nm. As the  $D$  of the array prepared via 40 V anodization was 95.44 nm (Fig. 5), UV reflection by the nanolens array might be specular, explaining the similar UV disinfections afforded by the electropolished aluminum and the nanolens array (Fig. 6A). Also, the extent of UV disinfection using the nanolens array prepared via 240 V anodization was no better than that of the electropolished aluminum, perhaps because of excessive UV diffusion. UV disinfection effectiveness enhancement by nanolens arrays seemed to be related to the  $D$  value. The  $D$  values of arrays prepared via 160 and 200 V anodization were similar, as were the UV disinfection results (Figs. 5 and 6A). The total UV doses to the water in the UV disinfection system might be the same when electropolished aluminum and nanolens arrays are used. However, the difference in UV disinfection was evident when the UV light was focused by the nanolens arrays. The UV light reflected by the

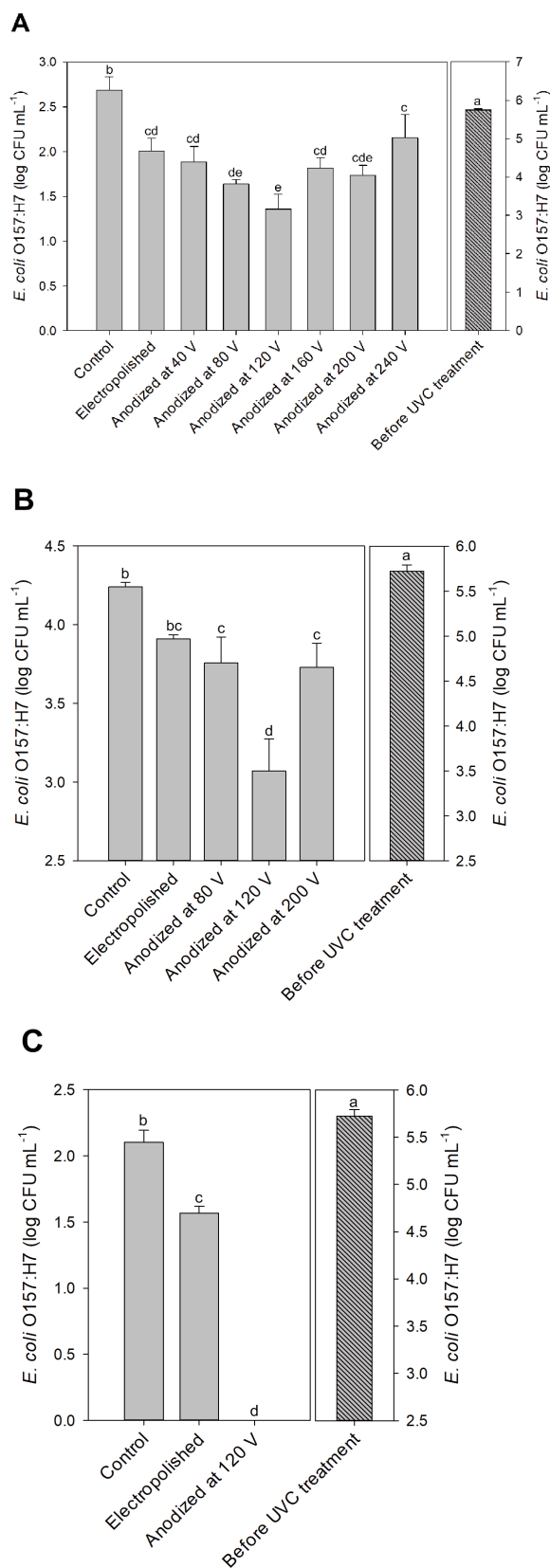


**Fig. 6.** UV disinfection test results when aluminum-based reflective nanolens arrays were employed. The flow rates of *E. coli* O157:H7-contaminated water were (A) 2, (B) 4, and (C) 1.5 mL s<sup>-1</sup>. Different letters above the error bars indicate significant differences ( $p < 0.05$ ) among the groups. UV, ultraviolet; *E. coli*, *Escherichia coli*.

nanolens array prepared via 120 V anodization may be better focused than that reflected by other nanolens arrays, enhancing UV disinfection effectiveness. Notably, the  $D$  of the nanolens array prepared via 120 V anodization was 226.64 nm, close to the wavelength of the irradiated UV (Figs. 5 and 6).

## CONCLUSION

UV water disinfection is dose-dependent. UV reflection behind irradiated water using electropolished aluminum and aluminum-based reflective nanolens arrays increased the UV dose to the water and enhanced the disinfection effectiveness compared to the non-reflective control system. Although the total UV doses applied were the same when the electropolished aluminum and aluminum-based reflective nanolens arrays were used, UV focusing by the nanolens arrays enhanced the disinfection effectiveness. The enhanced UV disinfection effectiveness was significant when an aluminum-based reflective nanolens array with  $D$  similar to the wavelength of the irradiated UV (245 nm) (i.e., an aluminum-based reflective nanolens array with  $D = 226.64$  nm prepared via 120 V anodization) was used. UV water disinfection system inevitably consumes electricity; therefore, the aluminum-based reflective nanolens array can be a means to save electricity consumed by the UV water disinfection system because it enhances disinfection without the need for additional electricity. Since UV rays have low penetration through organic and inorganic substances, UV irradiation is used to disinfect municipal and livestock water and sediment-removed municipal wastewater. The microbiological safety of livestock wastewater may be enhanced by applying a UV disinfection system combined with aluminum-based reflective nanolens arrays to sediment-removed livestock wastewater. However, it may be necessary to study a scaled-up aluminum-based reflective nanolens array-equipped UV disinfection system and investigate disinfection by the scaled-up system before application in livestock farms.

## REFERENCES

1. Carson TL. Current knowledge of water quality and safety for livestock. *Vet Clin N Am Food Anim Pract.* 2000;16:455-64. [https://doi.org/10.1016/S0749-0720\(15\)30080-3](https://doi.org/10.1016/S0749-0720(15)30080-3)
2. McAllister TA, Topp E. Role of livestock in microbiological contamination of water: commonly the blame, but not always the source. *Anim Front.* 2012;2:17-27. <https://doi.org/10.2527/af.2012-0039>
3. Bhagwat VR. Safety of water used in food production. In: Singh RL, Mondal S, editors. *Food safety and human health.* London: Academic Press; 2019. p. 219-47.
4. Frasier GW. Water harvesting. In: Fath BD, Jørgensen SE, Cole M, editors. *Managing water resources and hydrological systems.* 2nd ed. Boca Raton: CRC Press; 2020. p. 129-32.
5. van Eenige MJEM, Counotte GHM, Noordhuizen J. Drinking water for dairy cattle: always a benefit or a microbiological risk? *Tijdschr Diergeneeskd.* 2013;138:86-99.
6. Almashhadany DA. Meat borne diseases. In: Ranabhat CL, editor. *Meat and nutrition.* London: IntechOpen; 2021.
7. Allen MR, Dube OP, Solecki W, Aragón-Durand F, Cramer W, Humphreys S, et al. Framing and context. In: Masson-Delmotte V, Zhai P, Pörtner HO, Roberts D, Skea J, Shukla PR, et al., editors. *Global Warming of 15°C.* Cambridge and New York, NY: Cambridge University Press; 2018. p. 49-92.
8. Clarke B, Otto F, Stuart-Smith R, Harrington L. Extreme weather impacts of climate change: an attribution perspective. *Environ Res Clim.* 2022;1:012001. <https://doi.org/10.1088/2752->

- 5295/ac6e7d
9. Godde CM, Mason-D'Croz D, Mayberry DE, Thornton PK, Herrero M. Impacts of climate change on the livestock food supply chain; a review of the evidence. *Glob Food Secur.* 2021;28:100488. <https://doi.org/10.1016/j.gfs.2020.100488>
  10. Nikolaou AD, Kostopoulou MN, Lekkas T. Organic by-products of drinking water chlorination. *Glob Nest Int J.* 1999;1:143-56.
  11. Sciacca S, Conti GO. Mutagens and carcinogens in drinking water. *Mediterr J Nutr Metab.* 2009;2:157-62. <https://doi.org/10.1007/s12349-009-0052-5>
  12. DeMarini DM. A review on the 40th anniversary of the first regulation of drinking water disinfection by-products. *Environ Mol Mutagen.* 2020;61:588-601. <https://doi.org/10.1002/em.22378>
  13. Olkowski AA. *Livestock water quality: a field guide for cattle, horses, poultry and swine.* Ottawa: Agriculture & Agri-Food Canada; 2009. Cat. no.: A22-483/2009E
  14. Li X, Cai M, Wang L, Niu F, Yang D, Zhang G. Evaluation survey of microbial disinfection methods in UV-LED water treatment systems. *Sci Total Environ.* 2019;659:1415-27. <https://doi.org/10.1016/j.scitotenv.2018.12.344>
  15. Anil C, Rutuja D, Eswara P. Ultraviolet (UV) disinfection equipment market: global opportunity analysis and industry forecast, 2020–2027 [Internet]. Allied Market Research Report 2020. 2020 [cited 2022 Jul 7]. <https://www.alliedmarketresearch.com/UV-disinfection-equipment-market>
  16. Hijnen WAM, Beerendonk EF, Medema GJ. Inactivation credit of UV radiation for viruses, bacteria and protozoan (oo)cysts in water: a review. *Water Res.* 2006;40:3-22. <https://doi.org/10.1016/j.watres.2005.10.030>
  17. Kowalski W. UVGI disinfection theory. In: *Ultraviolet germicidal irradiation handbook: UVGI for air and surface disinfection.* Berlin, Heidelberg: Springer ; 2009. p. 17-50.
  18. Sommer R, Cabaj A, Haider T. Microbicidal effect of reflected UV radiation in devices for water disinfection. *Water Sci Technol.* 1996;34:173-7. <https://doi.org/10.2166/wst.1996.0619>
  19. Park J, Chai C. Aluminum based reflective nanolens arrays to improve the effectiveness of ultraviolet inactivation of *Escherichia coli* O157:H7 and *Listeria monocytogenes* in water and a sucrose solution. *Food Sci Biotechnol.* 2020;29:1281-7. <https://doi.org/10.1007/s10068-020-00765-z>
  20. Tortora GJ, Funke BR, Case CL. *Microbiology: an introduction.* 12th ed. San Francisco, CA: Pearson Education; 2015.
  21. Yaeger RG. Protozoa: structure, classification, growth, and development. In: Baron S, editor. *Medical microbiology.* 4th ed. Galveston, TX: University of Texas Medical Branch at Galveston; 1996.
  22. Hou Y, Li R, Liang J. Simultaneous electropolishing and electrodeposition of aluminum in ionic liquid under ambient conditions. *Appl Surf Sci.* 2018;434:918-21. <https://doi.org/10.1016/j.apsusc.2017.11.034>
  23. Ling Z, Li Y. Mechanisms of nanoporous alumina formation and self-organized growth. In: Losic D, Santos A, editors. *Nanoporous alumina: fabrication, structure, properties and applications.* Cham: Springer; 2015. p. 1-30.
  24. Keller F, Hunter MS, Robinson DL. Structural features of oxide coatings on aluminum. *J Electrochem Soc.* 1953;100:411. <https://doi.org/10.1149/1.2781142>
  25. Losic D, Santos A. *Nanoporous alumina: fabrication, structure, properties and applications.* Cham: Springer; 2015.
  26. Cheng C, Ngan AHW. Theoretical pore growth models for nanoporous aluminums. In: Losic

- D, Santos A, editors. Nanoporous alumina: fabrication, structure, properties and applications. Cham: Springer; 2015. p. 31-60.
27. Chu SZ, Wada K, Inoue S, Isogai M, Katsuta Y, Yasumori A. Large-scale fabrication of ordered nanoporous alumina films with arbitrary pore intervals by critical-potential anodization. *J Electrochem Soc.* 2006;153:B384. <https://doi.org/10.1149/1.2218822>
  28. Kikuchi T, Nakajima D, Nishinaga O, Natsui S, Suzuki RO. Porous aluminum oxide formed by anodizing in various electrolyte species. *Curr Nanosci.* 2015;11:560-71. <https://doi.org/10.2174/1573413711999150608144742>
  29. Zaraska L, Kurowska E, Sulka GD, Senyk I, Jaskula M. The effect of anode surface area on nanoporous oxide formation during anodizing of low purity aluminum (AA1050 alloy). *J Solid State Electrochem.* 2014;18:361-8. <https://doi.org/10.1007/s10008-013-2215-z>
  30. Lee SJ, Kim SJ. Effect of current density on porous film formation in two-step anodizing for Al alloy. *J Korean Inst Surf Eng.* 2016;49:125-9. <https://doi.org/10.5695/JKISE.2016.49.2.125>
  31. Gómez de Castro AI, Rheinstädter M, Clancy P, Castilla M, de Isidro F, Larruquert JI, et al. Graphite to diamond transition induced by photoelectric absorption of ultraviolet photons. *Sci Rep.* 2021;11:2492. <https://doi.org/10.1038/s41598-021-81153-3>
  32. Peiponen KE, Tsuboi T. Metal surface roughness and optical reflectance. *Opt Laser Technol.* 1990;22:127-30. [https://doi.org/10.1016/0030-3992\(90\)90022-V](https://doi.org/10.1016/0030-3992(90)90022-V)